Towards a measurement of the Debye length in very large Magneto-Optical traps

Julien Barre, R. Kaiser, G. Labeyrie, B. Marcos, D. Metivier

Towards a measurement of the Debye length in very large Magneto-Optical traps

J. Barré,[1] R. Kaiser,[2] G. Labeyrie,[2] B. Marcos,[3] and D. Métivier[3]

[1]*Institut Denis Poisson, Université d'Orléans, Université de Tours, CNRS, France, et Institut Universitaire de France*

[2]*Université Côte d'Azur, CNRS, Institut de Physique de Nice, 06560 Valbonne, France;*

[3]*Université Côte d'Azur, CNRS, Laboratoire J.-A. Dieudonné, 06109 Nice, France.*

(Dated: August 3, 2018)

We propose different experimental methods to measure the analog of the Debye length in a very large Magneto-Optical Trap, which should characterize the spatial correlations in the atomic cloud. An analytical, numerical and experimental study of the response of the atomic cloud to an external modulation potential suggests that this Debye length, if it exists, is significantly larger than what was expected.

PACS numbers:

I. INTRODUCTION

Magneto Optical Traps (MOTs), first realized in 1987 [1], are still an ubiquitous device to manipulate cold atoms. Early studies [2] have shown that when the number of trapped atoms is increased beyond a certain level, the peak density tends to saturate. This unwanted limitation to obtain high spatial densities of laser-cooled atomic samples has been attributed to an effective repulsion between atoms due to multiple scattering of photons. A basic model to describe atoms in a large MOT has then emerged, where atoms, beyond the friction and external trapping force, are subjected to two kinds of effective interaction forces: an effective Coulomb repulsion of [2], which is dominant, and an effective attraction, sometimes called shadow effect, first described in [3]. Even though the shortcomings of this model are well known (such as a too large optical depth, space dependent trapping parameters [4], sub-doppler mechanisms [5, 6], light assisted collisions [7] and radiative escape [8, 9] or hyperfine changing collisions [10, 11]), its predictions on the size and the shape of the atomic clouds are in reasonable agreement with experiments on very large MOTs [12].

It is striking that the above "standard model" describes MOTs as a kind of analog of a non neutral plasma, as well as an instance of an experimentally controllable system with long range interactions. This has prompted several studies [13–19], aimed at better probing this analogy and its consequences. We note that these long range forces stems from the resonant dipole-dipole coupling between atoms [20–26], which if interference can be neglected lead to radiation trapping of light in cold atoms [27–29]. This dipole-dipole coupling is also at the origin of modified radiation pressure on the center of mass [30, 31] and of optical binding with cold atoms [32] as weel as of super- an subradiance [33–35]

Current technologies now allow for larger and larger MOTs, for which long range interactions become even more important. Hence it becomes feasible to test more quantitatively this plasma analogy. In particular, spatial correlations in plasmas are controlled by a characteristic length, called the Debye length, which depends on charge, density, temperature. A natural question thus arises: is an experimental observation of a Debye length possible in a large MOT?

In this paper, we propose and analyze two types of experiments to probe spatial correlations in a MOT. We first present a direct measurement by diffraction, and highlight its inherent difficulties: we have not been able to measure spatial correlations this way. We demonstrate however that the cloud's response to an external modulation should provide an indirect measurement of the Debye length. Our experimental results then show that if the interactions are indeed adequately described by a Coulomb-like interaction, the corresponding Debye length is much larger than what could be expected based on the observed size of the cloud without interaction.

In section II, we present our experimental set-up, recall the basic features of the "standard model", based on [2], and discuss the relevant orders of magnitudes. In section III, we explain different options to probe the interactions and correlations inside the cloud: i) analysis of the density profile III A ii) direct diffraction experiments III B iii) response to an external modulation III C. While method ii) proves to be not viable with current techniques, comparison of analytical results, simulations and experiments for methods i) and iii) suggest that the Debye length in the cloud may be much larger than expected. The last section IV is devoted to a discussion of these results.

II. EXPERIMENTAL SETUP AND STANDARD THEORETICAL MODEL

A. Experimental setup

The experimental apparatus used in this work as been described in detail elsewhere [12]. ^{87}Rb atoms are loaded in a magneto-optical trap from a dilute room-temperature vapour. The trapping force is obtained by crossing six large laser beams (waist 2.4 cm) at the center of the vacuum chamber, arranged in a two-by-two counter-propagating configuration. These lasers are detuned from the $F = 2 \rightarrow \acute{F} = 3$ atomic transition of the D2 line by typically $\delta = -4\Gamma$, where Γ is the atomic linewidth. The peak intensity in each beam is 5 $\mathrm{mW/cm^2}$. The trapping beams also contain a small proportion (a few %) of "repumping" light, tuned close to the $F = 1 \rightarrow \acute{F} = 2$ transition. A pair of coils with opposite currents generate the quadrupole magnetic field necessary for trapping. The magnetic field gradient along the axis of the coils is 7.2 G/cm. Due to the large diameter of the trapping beams, the maximal number of trapped atoms is large, up to 10^{11}. As discussed in the following, this results in a large effective repulsive interaction between atoms mediated by scattered photons. As a consequence the cold atomic cloud is large with a FWHM diameter typically between 12 and 16 mm, depending on the value of δ. The temperature of the cloud is of the order 100-200 μK.

We now describe the various experimental techniques implemented to probe spatial correlations inside the atomic cloud. The results of these experiments and their comparison with theoretical models are presented in section III. The first technique simply relies on the analysis of the cloud's density profile. This is achieved by imaging the trapping light scattered by the atoms, known as "fluorescence" light, with a CCD camera. However, the spatial distribution of fluorescence light usually does not reflect that of the atomic density, because of multiple scattering [12]. To minimize this effect, we acquire the fluorescence image at a fixed detuning of -8Γ. The time sequence is as follows: the MOT is operating at a given detuning δ (variable), then the detuning is jumped to -8Γ for a duration of 10 μs, during which the image is recorded. During this short time, the atoms move only by a few 10 μm, which is much smaller than all spatial scales we look for.

The second technique is based on the direct diffraction of a probe beam by the cloud. A weak beam of waist 2.2 mm (much smaller than the cloud's diameter), detuned by several Γ, is sent through the center of the cloud immediately after the trapping beams are shut down. The transmitted far field intensity distribution is recorder using a CCD camera placed in the focal plane of a lens.

The third technique relies on the measurement of the cloud's response to an external sinusoidal modulation. Its principle is illustrated in Fig. 1. A sinusoidal potential is generated by crossing two identical laser beams of waist 2.2 mm and detuning +20Γ in the center of the cloud, with an adjustable small angle θ between them (Fig.1a). The resulting modulation period is $\lambda_e = \lambda/\theta$. The intensity of these beams is chosen low enough such that the associated radiation pressure force doesn't affect the functioning of the MOT (no difference in atom number with and without the modulation beams). To measure

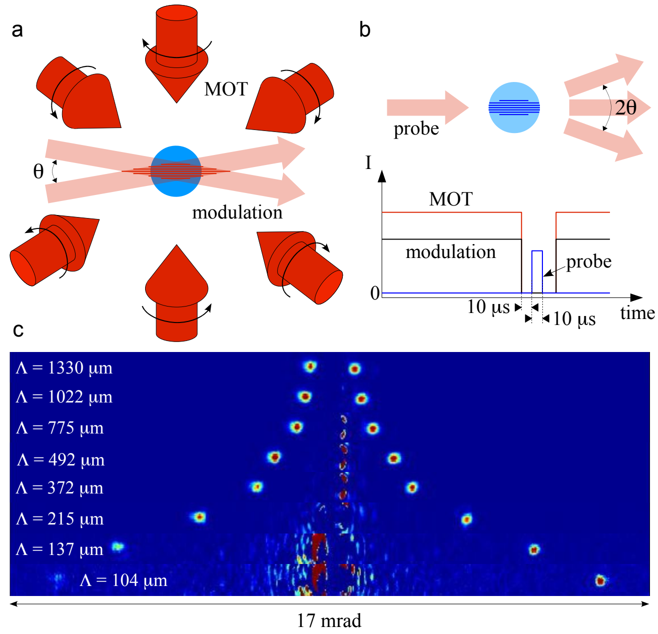

FIG. 1: Principle of modulation experiment. a: A sinusoidal modulation is applied by crossing two laser beams on the cloud. b: The atoms are released from the MOT and the diffraction grating due to the atomic density modulation is probed. c: Images of the ±1 diffracted orders versus modulation wavelength λ_e.

the response of the cloud (in the form of a density grating), we switch off the MOT laser beams and send the probe beam described before through the modulated part of the cloud. The short delay (10μs) between probing and MOT switching off ensures that the initial density modulation is not blurred by the residual atomic motion. The modulated atomic density acts for the probe as a transmission diffraction grating (Fig.1b). The zeroth and first diffracted orders are recorded by a CCD camera placed in the focal plane of a lens. Fig.1c shows the evolution of the separation 2θ between the $+1$ and -1 orders as λ_e is decreased (the zeroth order is blocked by a filter to avoid saturation of the CCD). In this figure, each image is displayed with a different intensity threshold to compensate for the decrease of diffraction efficiency with λ_e (see Fig.5).

B. Model

In the standard Doppler model, all forces on atoms inside a MOT stem from the radiation pressure exerted by the almost resonant photons. Over long enough time scales, the scattering of many photons produces an average force on the atomic cloud, which may be decomposed as: velocity trapping (ie friction), spatial trapping, attractive shadow effect, and repulsion due to multiple scattering. The first two are single atom effects, the last two are effective interactions between atoms. The friction force $F_{\rm dop}$ is due to Doppler cooling. Linearizing for small velocities, it reads

$$\vec{F}_{\rm dop} \simeq -m\gamma\vec{v}, \tag{1}$$

with

$$\gamma = \frac{I_0}{I_s}\frac{8\hbar k_{\rm Las}^2}{m}\frac{-\bar{\delta}}{\left(1+4\bar{\delta}^2\right)^2},$$

where $I_0, k_{\rm Las}, \bar{\delta} = \delta/\Gamma$ are respectively the laser intensity, wave number and scaled detuning, I_s is the saturation intensity, and m the atomic mass. This expression assumes a small saturation parameter. γ is positive (actual friction) when the lasers are red detuned ($\delta < 0$).

The trapping force $F_{\rm trap}$ is created by the magnetic field gradient. We will consider a linear approximation to this force:

$$\vec{F}_{\rm trap} \simeq -m\omega_x^2 x\vec{e}_x - m\omega_y^2 y\vec{e}_y - m\omega_z^2 z\vec{e}_z. \tag{2}$$

The antihelmhotz configuration of the coils induces a non isotropic trap, with $\omega_y^2 = \omega_z^2 = \frac{1}{2}\omega_x^2$. Nevertheless via laser intensity compensations it is possible to obtain a spherical cloud, hence we will use in our modelling $\omega_y = \omega_z = \omega_x = \omega_0$.

The shadow effect, first studied in [3], results from the absorptions of lasers by atoms with cross section σ_L in the cloud. The laser intensity decreases as the beam propagates into the cloud in direction $\vec{e}_z$ by a factor

$$e^{-b} = \exp\left(-\sigma_L\int_{-\infty}^{\infty}\rho(r_l')\,{\rm d}r_l\right)$$

where b is the optical depth of the cloud. Assuming $b \ll 1$, one may linearize the above exponential and obtain in direction x an effective force term:

$$\vec{\rm F}_{\rm s}[f](\vec{r})\cdot\vec{e}_x = -I_0\frac{\sigma_L^2}{c}\left(\int_{-\infty}^{x} - \int_{x}^{+\infty}\right)\rho(x',y,z)\,{\rm d}x'. \tag{3}$$

This force is attractive, and its divergence is

$$\vec{\nabla}\cdot\vec{\rm F}_{\rm s} = -6I_0\frac{\sigma_L^2}{c}\rho(x,y,z), \tag{4}$$

where c is the speed of light.

The repulsive force [2] is due to multiple scattering of photons. If the optical depth is small, very few photons are scattered more than twice, and the effect of multiple scattering can be approximated as an effective Coulomb repulsion

$$\vec{\rm F}_{\rm c}(\vec{r}) = 3I_0\frac{\sigma_L\sigma_R}{2\pi c}\frac{\vec{r}}{r^3}, \tag{5}$$

where σ_R is the atomic cross section for scattered photons. The divergence of the force is

$$\vec{\nabla}\cdot\vec{\rm F}_{\rm c} = 6I_0\frac{\sigma_L\sigma_R}{c}\rho(x,y,z)$$

The scattered photons actually have complex spectral and polarization properties, and σ_R should rather be understood as an averaged quantity. In all experiments, $\sigma_R > \sigma_L$, with the consequence that the repulsion dominates over the attractive shadow effect. Since repulsion and attraction both have a divergence proportional to the local density, the shadow effect is often considered as a mere renormalization of the repulsive force; note that this involves a further approximation, because the forces are not proportional, even though their divergences are.

Finally, the spontaneous emission of photons acts as a random noise on the atoms, which induces at the macroscopic level a velocity diffusion. Putting everything together, one obtains a Vlasov-Fokker-Planck equation for the atomic density in position and velocity $f(\vec{r},\vec{v},t)$

$$\partial_t f(\vec{r},\vec{v},t) = \vec{\nabla}\cdot\left(\omega_0^2\vec{r}\rho + \frac{1}{m}(\vec{\rm F}_{\rm c}+\vec{\rm F}_{\rm s})[\rho]\rho + \frac{k_{\rm B}T}{m}\vec{\nabla}\rho\right), \tag{6a}$$

and a Poisson equation for the force

$$\vec{\nabla}\cdot(\vec{\rm F}_{\rm c}+\vec{\rm F}_{\rm s}) = C\rho \text{ with } C = 6I_0\frac{\sigma_L(\sigma_R-\sigma_L)}{c}. \tag{6b}$$

This is a simplified version of the Fokker-Planck equation in [36]. In our experiments, the atomic dynamics is typically overdamped: the velocity damping time is much shorter than the position damping time. The velocity distribution then quickly relaxes to an approximate gaussian, and the density distribution is described by the Smoluchowsky equation:

$$\partial_t\rho(\vec{r},t) = \vec{\nabla}\cdot\left(\omega_0^2\vec{r}\rho + \frac{1}{m}(\vec{\rm F}_{\rm c}+\vec{\rm F}_{\rm s})[\rho]\rho + \frac{k_{\rm B}T}{m}\vec{\nabla}\rho\right), \tag{7}$$

while (6b) is not modified. Note finally that in this simplified framework the total force $\vec{\rm F}_{\rm c}+\vec{\rm F}_{\rm s}$ has the same divergence as an effective Coulomb force

$$\tilde{\vec{F}}_c(\vec{r}) = \frac{C}{4\pi}\frac{\vec{r}}{r^3}. \tag{8}$$

C. Analysis of the model

The above model describes a large MOT as a collection of particles in a harmonic trap, and the dominant interacting force is a Coulomb-like repulsion. This clearly suggests an analogy with non neutral plasmas, where trapped electrons interact through real Coulomb forces; for a detailed review, see [37]. The analogy is not perfect: for instance the non potential part of the shadow effect is neglected, the friction and diffusion in a MOT are much stronger than in a non neutral plasma, and the typical optical depth in an experiment is not very small. Nevertheless, it is a basic model to analyze MOT physics, and has been used recently to predict new plasma related phenomena in MOTs (see for instance [16, 38]).

a. Temperature and repulsion dominated regimes When the repulsion force is negligible, the trapping force is balanced by the temperature. The cloud has then a gaussian shape, with atomic density

$$\rho(\vec{r}) = \frac{N}{(2\pi l_g^2)^{3/2}} e^{-\frac{\vec{r}^2}{2l_g}} \ , \text{ with } l_g = \left(\frac{k_B T}{m\omega_0^2}\right)^{1/2} \ , \quad (9)$$

where N is the total number of trapped atoms. In the following, l_g will be called the "gaussian length". For typical MOT parameters, one has as an order of magnitude $l_g \sim 200\mu m$. Increasing N, the repulsion increases, and the system enters the repulsion dominated regime, where the trapping force is balanced by the repulsion. Theory then predicts a spherical cloud with constant density ρ_c, and step-like boundaries smoothed over the same length scale l_g defined in Eq. (9) [37]; the typical size of the cloud is denoted by L, and we have the expressions

$$\rho_c = \frac{3m\omega_0^2}{C} = \frac{3m\omega_0^2 c}{6I_0\sigma_L(\sigma_R - \sigma_L)} \ , \ L \sim \rho_c^{-1/3} N^{1/3}. \quad (10)$$

The cross over between temperature and repulsion dominated regimes is for $l_g \sim L$. Experimentally, sizes of order $L \sim 1\,\text{cm}$ can be reached (see section II A), which should be well into the repulsion dominated regime. Note that the repulsion dominated regime is not as straightforward to analyze when the trap anisotropy and shadow effect are taken into account, see [39].

b. Plasma coupling parameter and Debye length To quantify the relative effect of kinetic energy and Coulomb repulsion, it is customary for plasmas to define the "plasma coupling parameter" Γ_p, which is the ratio of the typical potential energy created by a neighboring charge by the typical kinetic energy. For a MOT in the repulsion dominated regime, denoting $a = (3\rho_c/4\pi)^{-1/3}$ a measure of the typical interparticle distance, we have the expression

$$\Gamma_p = \frac{C/(4\pi a)}{k_\text{B}T} = \frac{a^2}{l_g^2} \quad (11)$$

where we have used (10), and we recall that $l_g = (k_B T/m\omega_0^2)^{1/2}$ is the "gaussian length". Using typical experimental values $l_g = 200\mu m$, and an atomic density $\rho = 10^{11}\text{cm}^{-3}$, this yields $\Gamma_p \sim 10^{-4}$. A plasma experiences a phase transition from liquid phase to solid phase at $\Gamma_p \simeq 175$, and is considered in a gas-like phase as soon as $\Gamma_p < 1$. The typical value for a MOT experiment is hence very small, well into the gas phase, and the expected correlations are weak. In this regime, and assuming the MOT shape is dominated by repulsion, so that the density in the central region is approximately constant, Debye-Hückel theory then yields for the pair correlation function [40]

$$g^{(2)}(r) = \exp\left(-a\frac{\Gamma_p}{r}e^{-r/\lambda_D}\right) \ , \text{ with } \lambda_D = \left(\frac{k_B T}{\rho_c C}\right)^{1/2}. \quad (12)$$

This expression assumes isotropy: this is why the correlation depends only on one distance r. $g^{(2)}$ vanishes for small r, which is a manifestation of the strong repulsion, and tends to 1 for $r \gg \lambda_D$, $g^{(2)} \simeq 1$: correlations disappear in this limit. The excluded volume effect kicks in at very small scales, of order $a\Gamma_p$; at larger scales, the above expression can be replaced by:

$$g^{(2)}(r) \simeq 1 - \frac{a\Gamma_p}{r}e^{-r/\lambda_D} \ . \quad (13)$$

Inserting the expression for ρ_c (10), one obtains the expression $\lambda_D = l_g/\sqrt{3}$, and the rough order of magnitude $\lambda_D \sim 100\mu m$. Using this and the estimated Γ_p in (13), we see that the correlations are indeed very small over length scales of order λ_D.

D. Experimental probes of the "Coulomb" model

Following [2], describing the optical forces induced by multiple scattering as an effective Coulomb repulsion is a standard procedure since the early 90s. In particular, it satisfactorily explains the important observation that the atomic density in a MOT has an upper limit (preventing for instance the initially sought Bose-Einstein condensation). However other mechanisms can lead to a upper density, such as light assisted collisions or other short range interactions [7, 9, 41]. Besides the bounded density, are experiments are consistent with a Coulomb type repulsion:

- The size scaling $L \sim N^{\sim 1/3}$ was observed with reasonable precision in experiments [12, 42–44]; however, this is not a unique signature of a Coulomb repulsion as other repulsive forces (e.g. short ranged inetractions) can lead to a saturation of the spatial density.

- A Coulomb explosion in a viscous medium has been observed by measuring the expansion speed of a cold atomic cloud in optical molasses: [13, 45]. The result shows a good agreement with what is predicted for a similar Coulomb gas.

- Self-sustained oscillations of a MOT have been reported in [14]. The model used to explain the experimental observations assume a cloud with a size increasing with the atom number. This is again consistent witht a Coulomb type repulsion but remains a indirect test of these forces.

All these experiments rely on identifying macroscopic effects of the repulsive force, and microscopic effects such as the building of correlations in the cloud have not been directly observed. This is our goal in the following.

III. LOOKING FOR CORRELATIONS IN EXPERIMENTS

In order to measure directly or indirectly the interaction induced correlations in the atomic cloud, we have performed three types of experiments, which rely on: i) an analysis of the density profile, ii) a direct measurement of correlations by diffraction iii) an analysis of the cloud's response to an externally modulated perturbation. This section gathers our results.

A. Analysis of the density profile

From the theoretical analysis presented in the previous section, we know that our basic model (7) relates the Debye length λ_D, which controls the correlations, to the "gaussian length" l_g, which controls the tails of the density profile: $\lambda_D = l_g/\sqrt{3}$. Fitting the experimental density profile may then provide information on the Debye length. We recall that this is an indirect method and only serves a a guide for an more reliable estimation of the Debye length.

The experimental data obtained by fluorescence [12]) is two dimensional, since the density is integrated over one direction (called z below); selecting the central part $y \in [-\epsilon, \epsilon]$, where ϵ is about 10% of cloud's width, we obtain the observed density along the x direction:

$$\rho_x(x) = \int_{-\infty}^{\infty} \mathrm{d}z \int_{-\epsilon}^{\epsilon} \mathrm{d}y \ \rho(x, y, z),$$

Figure 2 shows, for two values of the detuning δ, this partially integrated experimental density profile ρ_x.

We compare these profiles with Coulomb Molecular Dynamics (MD) simulations. We use $N = 16384$ particles in an harmonic trap interacting through Coulombian interactions (without shadow effect) with friction and diffusion, as presented in (7) and (17). We use a second order Leap-Frog scheme (see e.g. [46]); the interaction force is implemented in parallel on a GPU. We use a time step of $\Delta t = 10^{-5}$. We choose the parameters L and λ_D to match the experimental density. Knowing the simulation parameters allows us to deduce the gaussian length l_g. Figure 2 shows that the fits are reasonably good, and allow to extract a value for the Debye length λ_D and the cloud's size in the zero temperature limit L. These results suggest a value for the Debye length in the $1 - 2$mm range, much larger than what was expected on the basis of the experiments in the temperature dominated regime, see section II. However, this method is very model dependent: one could imagine other physical mechanisms or interaction forces producing similar density profiles. To overcome this difficulty, we need methods able to probe more directly the interaction and correlations inside the cloud. This is the goal of Sections III B and III C.

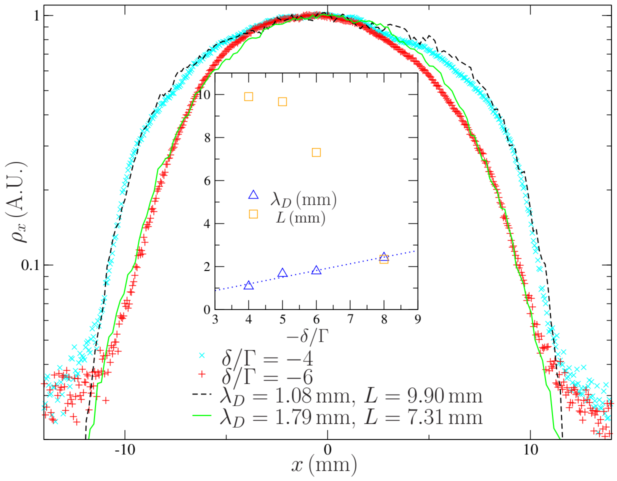

FIG. 2: Density $\rho_x(x)$ obtained by fluorescence for $-\delta/\Gamma = 4, 6$ compared with MD simulation of a trapped Coulomb gas, using $N = 16384$ particles. The inset shows the extrapolated Debye length λ_D and the cloud radius L. (The density plots for $-\delta/\Gamma = 5, 8$ are not shown here).

B. Direct probing of correlations by diffraction

An alternative method to probe spatial correlations of particles and thus access the Debye length is by directly probing two-body correlations via a diffraction experiment: an additional detuned laser beam is sent through the cloud, and the diffracted intensity I is recorded. For an incident plane wave, I is proportional to the structure factor [40]

$$S(\vec{k}) = \left\langle \frac{1}{N} \hat{\rho}(\vec{k}) \hat{\rho}(-\vec{k}) \right\rangle = \left\langle \frac{1}{N} \left| \sum_i e^{-i\vec{k}\cdot\vec{r}_i} \right|^2 \right\rangle \quad (14)$$

where the bracket stands for the ensemble average and $\vec{k} = \vec{k}_{\text{inc}} - \vec{k}_{\text{end}}$ is the difference between the incident wavevector $\vec{k}_{\text{inc}} = k_i \vec{e}_z$ and the diffracted one $\vec{k}_{\text{end}} = k_i(\cos\phi_k \sin\theta_k, \sin\phi_k \sin\theta_k, \cos\theta_k)$; this assumes elastic scattering, see figure 3.

We then have

$$k = |\vec{k}| = 2k_i \sin(\theta_k/2). \quad (15)$$

In an isotropic homogeneous infinite medium the structure factor can be computed explicitly using (13) [40]:

$$S(k) = N\delta(k) + \frac{k^2}{k^2 + \kappa_D^2} \quad (16)$$

with $\kappa_D = 1/\lambda_D$. The Dirac function corresponds to the unscattered radiation. For weak plasma parameter $\Gamma_p \to 0$, particles are uncorrelated and Poisson distributed; there is no characteristic correlation length, $\lambda_D \to \infty$ and the structure factor is constant

$$S = N\delta(k) + 1.$$

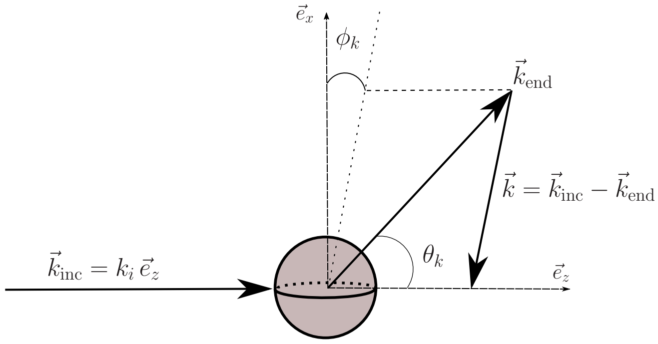

FIG. 3: Sketch of an incident beam $\vec{k}_{\rm inc}$ diffracted on an atom in direction $\vec{k}_{\rm end}$ corresponding to angles θ_k and ϕ_k. We define and show the vector $\vec{k} = \vec{k}_{\rm inc} - \vec{k}_{\rm end}$.

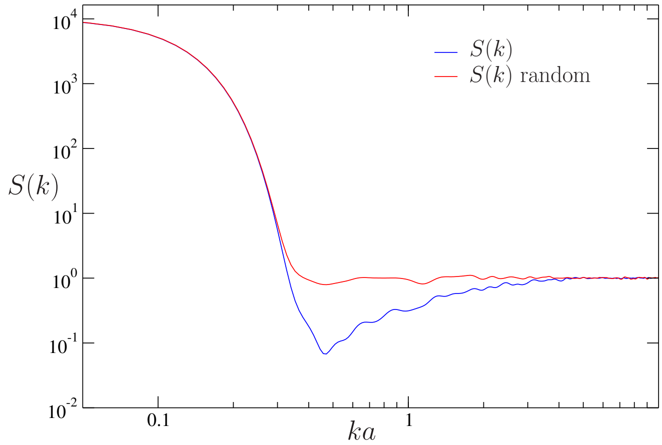

FIG. 4: MD simulations with $N = 16384$ particles of the structure factor $S(k)$, averaged over all $\vec{k}$ such that $|\vec{k}| = k$. The horizontal axis is adimensionalized by the mean inter-particle distance a, which is in the simulation $a/L = 0.039$. The parameters for the blue curve are: $\lambda_D/L \simeq 4.9\ 10^{-2}$, $\Gamma_p \simeq 0.215$ (this value for the plasma parameter is much higher than expected in the atomic coud; smaller, more realistic, values are difficult to reach numerically while keeping a small λ_D/L). The waist of the gaussian probe beam is $w \simeq 0.76L$. The red curve correspond to randomly distributed particles with the same average density: the two-body correlation obviously vanishes in this case, and accordingly, the characteristic dip is absent.

In the actual experiment, the structure factor (16) is modified at small k either by the finite size of the cloud, or by the finite waist of the probe beam, whichever is smaller: the resulting central peak then simply reflects the Fourier transform of the density profile or of the beam profile. Figure 4 shows an example of $S(k)$ for an MD simulation of a trapped Coulomb cloud, with a gaussian probe beam smaller than the cloud:

- The main peak $S(k=0) = N$ corresponds to the unscattered radiation.
- For small $k \sim 1/L$, there is a large smooth peak, corresponding to the Fourier transform of the probe beam's profile.
- For large k, the structure factor tends to 1.
- For intermediate $k \sim 1/\lambda_D$, there is a small dip which is the manifestation of the Debye length. It is deeper when the temperature is smaller, since correlations are stronger. It disappears for large temperature (the red curve in Fig. 4 formally corresponds to an infinite temperature).

Unfortunately, it is difficult to disentangle the small dip, signature of the Debye length, from the tails of the central peak, related to the finite cloud's size: we have not been able to reach a sufficient signal to noise ratio. This is coherent with the results of Sect. III A, which indicate that the size of the cloud L is not much larger than the Debye length λ_D.

C. Response to an external modulation

1. *Principle of the experiment and set-up*

Since a direct measure of correlations inside the cloud is currently not accessible, we have studied indirectly the effect of these correlations, by analyzing the response to an external force. As we will see in III C 2, this response is related to the interactions inside the cloud.

2. *Theoretical analysis: Bragg and Raman-Nath regimes*

The static modulation potential in the direction $\vec{e}_x$, with amplitude A, reads:

$$\phi_{\rm ext} = A\sin(k_e x). \tag{17}$$

Writing the new density profile as a perturbation around the constant density ρ_c, $\rho(\vec{r}) = \rho_c + \delta\rho(\vec{r})$, we can compute $\delta\rho$ at linear order from (7) (this neglects the effect of the cloud's boundary):

$$\delta\rho(x,y,z) = \frac{A}{k_{\rm B}T}\rho_c B(k_e)\sin(k_e x) \tag{18}$$

where

$$B(k_e) = \frac{k_e^2}{k_e^2 + \kappa_D^2}$$

is the response function. Hence the modulated profile has a clear amplitude dependence on the modulation number k_e and it is characteristic of Coulomb interactions (another force would have given a different result). When the modulation wavelength is increased beyond the Debye length ($L > \lambda_e > \lambda_D$), the response decreases, which means that large scale inhomogeneities are more difficult to create: this is an effect of repulsive long range interactions. Therefore, measuring this response function should provide information on the interactions inside the cloud.

The density modulation of the cloud is measured by diffraction: the diffracted amplitude at wavenumber $\vec{k}_e$ is related to the response function $B(k_e)$. However, this relationship is not straightforward. In particular, we shall see now that there are two distinct diffraction regimes, Bragg at small wavelength, and Raman-Nath at large wavelength.

The diffraction profile is proportional to the structure factor, which is for the modulated cloud:

$$S(\vec{k}) = S^0(\vec{k}) + \frac{2}{N}\delta\hat{\rho}(\vec{k})\hat{\rho}^0(\vec{k}) + \delta\hat{\rho}(\vec{k})^2 + \mathrm{O}\left(\text{correlation}\right), \tag{19}$$

where S^0 is the structure factor of the cloud without external modulation; we will neglect the correlations because they are very small as we have seen in section III B. The Fourier transform of the modulated cloud $\delta\hat{\rho}(\vec{k})$ can be related to the Fourier transform of the unperturbed cloud $\hat{\rho}^0(\vec{k})$, taking into account the shift in $\vec{k}$ induced by the $\sin(k_e x)$ function $k_x \to k_x \pm k_e$. The diffracted peaks correspond to maxima of the structure factor and are situated around the wavenumber $|\vec{k}| \simeq |\vec{k}_e|$. To compute their amplitude and shape one can expand in (19) around $k = k_e$, and $\phi_k = 0$ or π (these two angles correspond experimentally to the two diffraction peaks observed, see Fig. 3 for definition of k and ϕ_k).

We probe a wavenumber region $k_e \in [\sim 10^3, \sim 10^5]\,\mathrm{m}^{-1}$, with $k_i = 2\pi\frac{10^6}{0.78}\,\mathrm{m}^{-1}$, so that $k_e/k_i \ll 1$. This justifies the following expansion

$$\begin{aligned}|k_e\,\vec{e}_k - k_e\,\vec{e}_x| &= \frac{k_e^2}{2k_i} + k_e \times \mathrm{O}\left(\left(\frac{k_e}{2k_i}\right)^2\right) \\ &\simeq k_z \neq 0.\end{aligned} \tag{20}$$

In the perturbed density profile, it yields at the diffracted peak $k \simeq k_e$

$$\hat{\rho}(k_e) \simeq \hat{\rho}^0(k_e) - \frac{A}{2k_\mathrm{B}T}B(k_e)\left(\hat{\rho}^0\left(2k_e\right) - \hat{\rho}^0\left(\frac{k_e^2}{2k_i}\right)\right). \tag{21}$$

Since $\hat{\rho}(k=0) = N$ and the Fourier transform of the profile decreases very quickly to 0 with increasing k (the more regular $\rho(r)$ is, the faster its Fourier transform goes to 0) the dominant term in (21) is the last one, provided $NA/(k_\mathrm{B}T) \gg 1$ (this is typically the case in experiments) and $k_e \gtrsim 1/L$. Hence the diffracted peak maximum intensity is given by

$$S(k_e) \simeq 1 + \frac{1}{N}\left(\frac{A}{2k_\mathrm{B}T}\right)^2 B^2(k_e)(\hat{\rho}^0(k_z))^2. \tag{22}$$

Thus the diffraction response depends on the longitudinal density profile and not only on the response function $B(k_e)$. The density dependence crossovers at $k_z L \sim 1$, which defines a critical modulation wavelength $\lambda_e^{(c)}$ (or wavenumber $k_e^{(c)}$)

$$\lambda_e^{(c)} = 2\pi\sqrt{\frac{L}{2k_i}} = \sqrt{\pi L\lambda_i} \quad \text{or} \quad k_e^{(c)} = \sqrt{\frac{2k_i}{L}}. \tag{23}$$

It separates on one side the Raman-Nath regime $k_z L \ll 1$, where the diffracted peak intensity depends only on the response function, and on the other side the Bragg regime $k_z L \gtrsim 1$, where $\hat{\rho}^0(k_z)$ is not constant and decreases quickly to zero. Thus in this latter regime there is an additional dependence related to the Fourier transform of the density profile, that we call "density effect". Note that in the context of ultrasonic light diffraction this criterion (23) separating Bragg and Raman-Nath regimes is also known [47]. For a cloud of radius $L \approx 6\,\mathrm{mm}$ and a laser $\lambda_i \simeq \lambda_L = 780\,\mathrm{nm}$, the crossover is expected around $\lambda_e^{(c)} \approx 120\,\mu\mathrm{m}$.

It must also be noted that the experimentally measured quantity is not the peak amplitude $S(k_e)$, but rather the diffracted power $R(k_e)$: this brings an extra dependence on k_e. To simply show this, one can expand the structure factor around the peak and, assuming for instance a Gaussian shape around the maximum, deduce a linear dependence on the modulation wavelength $\lambda_e = 2\pi/k_e$ (the precise form of the shape around the maximum does not modify this linear dependence). To summarize, we expect to measure

$$R(k_e) \propto B^2(k_e) \times \begin{cases}\lambda_e(\hat{\rho}^0(\lambda_i\pi/\lambda_e))^2, & \lambda_e \ll \lambda_e^{(c)} \\ \lambda_e, & \lambda_e^{(c)} \ll \lambda_e \ll L.\end{cases} \tag{24}$$

In this expression, both the density dependence and response function $B(k_e)$ are a priori unknown. In order to obtain a well defined theoretical prediction, we assume for the cloud's profile a symmetrized Fermi function [48], ie a step smoothed over a length scale l. In the direction perpendicular to the probing beam, the cloud is effectively limited by the waist of the probing laser w; we assume a gaussian laser profile. This yields a simplified density profile

$$\rho(r_\perp, z) \propto \frac{l}{L}\frac{\sinh\left(\frac{L}{l}\right)}{\cosh\left(\frac{L}{l}\right) + \cosh\left(\frac{z}{l}\right)}\exp\left(-\frac{2r_\perp^2}{w^2}\right). \tag{25}$$

Its associated structure factor can be evaluated analytically thanks to [48]. Putting together all the results of this section, we obtain the theoretical predictions shown on Fig.5.

a. Comparison In Figure 5 we plot the result of an experiment for a detuning $\delta = -3\Gamma$. We compare these results with the theoretical diffraction response of the profile (25). The parameters L, w, N are chosen to be the same as in the experiment. Indeed, the waist w and atom number N are well controlled and the size of the cloud L can be extracted from a density profile. The smoothing length l appearing in (25) is chosen in the range suggested by the density profiles, see Fig. 2, and does not have much influence on the results. The only adjusted parameter here is the vertical amplitude of the theoretical response (in arbitrary units), that we set so it coincides with the experimental curves. The three theoretical curves correspond to three values for the Debye length λ_D: this modifies the response function B.

The conclusions of this comparison are

- The Bragg/Raman-Nath crossover predicted in (23) is observed in the experiment, at the predicted location.
- In the Bragg regime the theoretical response is smaller than what is observed. In this region, the response is sensitive to the details of the density profile, and our simple assumption (25) may not be good enough.
- The theoretical analysis predict oscillations in the Bragg regime. While these oscillations are not clearly resolved in the experiments, some hints are visible on figure 5 (vertical dashed lines around $\lambda_e = 70\,\mu$m). In the next paragraph, we analyze in more details the theoretical and experimental diffraction profiles, to confirm that the experimental observations are indeed a remnant of the theoretically predicted oscillations.
- In the Raman-Nath regime close to the crossover, the slopes of experiment and theory are both about 1. For larger modulation wavelength, we expect the long-range effects to take place. We indeed see clearly on the theoretical curve with $\lambda_D = 100\,\mu$m a decreasing response. For $\lambda_D = 300\,\mu$m this decrease occurs for larger λ_e and is thus barely visible. For comparison, we plot (blue dashed line) the limit $\lambda_D \to \infty$, corresponding to a non interacting case.

  The experimental data show no decrease for large wavelength: hence they are close to the "no interaction" case. More precisely, these data match the Coulomb predictions only if the Debye length is larger than $\sim 400\,\mu$m. Unfortunately, probing larger λ_e is difficult and would be hampered by strong finite size effects.

b. Oscillations in the Bragg regime In the Bragg regime, the shape of the diffracted beams observed in the experiment shows some variations, as seen on Figure 6(b): for $\lambda_e = 75.7\mu m$, the diffracted beam is split in two. Can we explain this observation? One has to remember that the response depends on the longitudinal profile (21); thus around a peak $k = k_e + \delta k$, the response is

$$S(k) \propto S^0\left(\frac{k_e^2 + 2k_e\delta k}{2k_i}\right).$$

If this small angle happens to correspond to a "hole" in the Fourier profile (as in Figure 4 for $ka < 1$), then the diffracted beam can be split in two parts. We illustrate this with our theoretical model with parameters

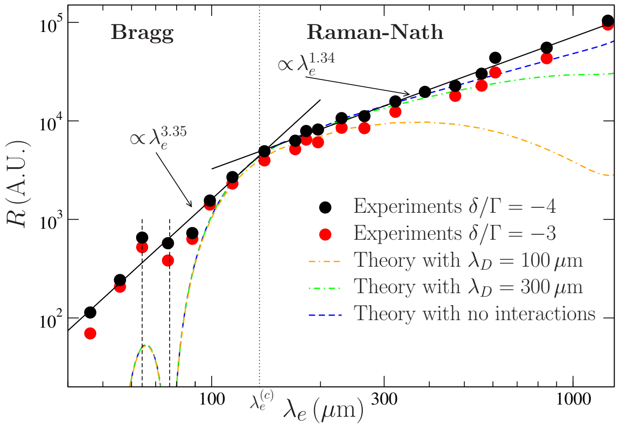

FIG. 5: Comparison of the total diffracted power $R(\lambda_e)$ in the experiment (crosses) and theory (lines). The detuning is $\delta/\Gamma = -3$, $N \sim 10^{10}$, $L = 7.41\,$mm, $w = 2.2\,$mm. We compare the theoretical model with the same parameters L, w, and changing the Debye length $\lambda_D = 100, 300\,\mu$m. The steepness l of the step function in (25) is chosen to be $l = 1$mm (the theoretical curve only weakly depends on l). We also show the theoretical limit case with no interactions $B(\lambda_e) = 1$. The vertical dotted line indicates the theoretical position of the theoretical Bragg/Raman-Nath cross-over $\lambda_e^{(c)} = 136\,\mu$m. The corresponding experimental value $\lambda_e^{(c),\mathrm{exp}} = 142\,\mu$m is obtained at the intersection of the fitted experimental data (for $\delta/\Gamma = -4$) in the Bragg $\propto \lambda_e^{3.35}$ and Raman-Nath region $\propto \lambda_e^{1.34}$.

provided by the experiments (there is no fit). We can see in Figure 5, (dashed lines) that a split beam is also expected around $\lambda_e = 76.5\,\mu$m. We show the corresponding beam shape in figure 7(b). In Figure 6(a) we show an experimental image for $\lambda_e = 64.2\,\mu$m (see the left vertical dashed line of Figure 5) where no splitting is expected. There is indeed no particular asymmetry and the beam is circular, in agreement with the theoretical prediction Fig. 7(a), not split. This analysis provides a satisfactory explanation of the experimental observation, and suggests that the Bragg regime is well understood.

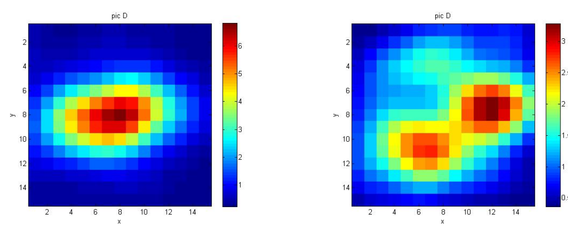

(a)$\lambda_e = 64.2\,\mu$m (b)$\lambda_e = 75.7\,\mu$m

FIG. 6: Experimental diffracted beams for $\lambda_e = 64.2$ and $75.68\,\mu$m.

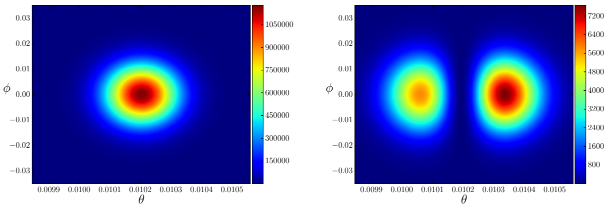

(a)$\lambda_e = 64.2\,\mu$m (b)$\lambda_e = 76.5\,\mu$m

FIG. 7: Theoretical diffracted beams for $\lambda_e = 64.2$ and $75.68\,\mu$m.

IV. CONCLUSION

We have proposed in this paper to use the response to an external modulation as an indirect way to measure the correlations inside the atomic cloud, and more generally to probe the effective interactions induced by the multiple photon scattering in large MOTs.

The modulation experiments and comparison with simulations did not show any evidence for a Debye length within the explored range, which could indicate a larger than expected value for λ_D of at least 400 μm for a detuning $\bar{\delta} = -4$. This seems consistent with direct numerical fits of the cloud's density profile, which suggest a Debye length as large as 1 mm. Accordingly, an extension of the modulation experiment to larger wavelengths could be envisioned. These values should be compared to the rough a priori estimate $\lambda_D \sim 100$ μm, based on the Coulomb model for the interaction between atoms and the observed size of the cloud. A clear theoretical explanation for the discrepancy between the a priori estimate for λ_D and the bounds provided by the experiments is lacking. It is possible that the Coulomb model for the effective interactions between atoms reaches its limits in such large MOTs: the Coulomb approximation relies on a small optical depth, whereas it is around 1 in experiments; or the spatial dependencies of the scattering sections may have to be considered. In either case, a refined model taking these effects into account would be considerably more complicated. It might also be that another mechanism controlling the maximum density, and hence the size of the cloud, is at play beyond multiple diffusion.

[1] E. L. Raab, M. Prentiss, A. Cable, S. Chu, and D. E. Pritchard, Physical Review Letters **59**, 2631 (1987), URL `https://link.aps.org/doi/10.1103/PhysRevLett.59.2631`.

[2] T. Walker, D. Sesko, and C. Wieman, Physical Review Letters **64**, 408 (1990).

[3] J. Dalibard, Optics Communications **68**, 203 (1988), ISSN 0030-4018, URL `http://www.sciencedirect.com/science/article/pii/003040188890185X`.

[4] C. Townsend, N. Edwards, C. Cooper, K. Zetie, C. Foot, A. Steane, P. Szriftgiser, H. Perrin, and J. Dalibard, Physical Review A **52**, 1423 (1995).

[5] J. Dalibard and C. Cohen-Tannoudji, JOSA B **6**, 2023 (1989), ISSN 1520-8540, URL `https://www.osapublishing.org/abstract.cfm?uri=josab-6-11-2023`.

[6] K. Kim, H.-R. Noh, H.-J. Ha, and W. Jhe, Physical Review A **69**, 033406 (2004).

[7] J. Weiner, V. S. Bagnato, S. Zilio, and P. S. Julienne, Rev. Mod. Phys. **71**, 1 (1999), URL `https://link.aps.org/doi/10.1103/RevModPhys.71.1`.

[8] C. C. Bradley, J. J. McClelland, W. R. Anderson, and R. J. Celotta, Phys. Rev. A **61**, 053407 (2000), URL `https://link.aps.org/doi/10.1103/PhysRevA.61.053407`.

[9] A. R. L. Caires, G. D. Telles, M. W. Mancini, L. G. Marcassa, V. S. Bagnato, D. Wilkowski, and R. Kaiser, Brazilian Journal of Physics **34**, 1504 (2004), ISSN 0103-9733, URL `http://www.scielo.br/scielo.php?script=sci_arttext&pid=S0103-97332004000700031&nrm=iso`.

[10] D. Sesko, T. Walker, C. Monroe, A. Gallagher, and C. Wieman, Phys. Rev. Lett. **63**, 961 (1989), URL `https://link.aps.org/doi/10.1103/PhysRevLett.63.961`.

[11] H. J. Lee, C. S. Adams, M. Kasevich, and S. Chu, Phys. Rev. Lett. **76**, 2658 (1996), URL `https://link.aps.org/doi/10.1103/PhysRevLett.76.2658`.

[12] A. Camara, R. Kaiser, and G. Labeyrie, Physical Review A **90**, 063404 (2014), URL `http://link.aps.org/doi/10.1103/PhysRevA.90.063404`.

[13] L. Pruvost, I. Serre, H. T. Duong, and J. Jortner, Physical Review A **61**, 053408 (2000), URL `http://link.aps.org/doi/10.1103/PhysRevA.61.053408`.

[14] G. Labeyrie, F. Michaud, and R. Kaiser, Physical Review Letters **96**, 023003 (2006), URL `https://link.aps.org/doi/10.1103/PhysRevLett.96.023003`.

[15] T. Pohl, G. Labeyrie, and R. Kaiser, Phys. Rev. A **74**, 023409 (2006), URL `https://link.aps.org/doi/10.1103/PhysRevA.74.023409`.

[16] J. Mendonça, R. Kaiser, H. Terças, and J. Loureiro, Physical Review A **78**, 013408 (2008).

[17] J. Mendonça and H. Terças, Journal of Physics B: Atomic, Molecular and Optical Physics **44**, 095301 (2011).

[18] H. Terças, J. T. Mendonça, and R. Kaiser, EPL (Europhysics Letters) **89**, 53001 (2010), ISSN 0295-5075, URL `http://stacks.iop.org/0295-5075/89/i=5/a=53001`.

[19] J. T. Mendonça and R. Kaiser, Phys. Rev. Lett. **108**, 033001 (2012), URL `https://link.aps.org/doi/10.1103/PhysRevLett.108.033001`.

[20] Courteille, Ph. W., Bux, S., Lucioni, E., Lauber, K., Bienaimé, T., Kaiser, R., and Piovella, N., Eur. Phys. J. D **58**, 69 (2010), URL `https://doi.org/10.1140/epjd/e2010-00095-6`.

[21] T. Bienaimé, M. Petruzzo, D. Bigerni, N. Piovella, and R. Kaiser, Journal of Modern Optics **58**, 1942 (2011), https://doi.org/10.1080/09500340.2011.594911, URL

https://doi.org/10.1080/09500340.2011.594911.

[22] L. Chomaz, L. Corman, T. Yefsah, R. Desbuquois, and J. Dalibard, New Journal of Physics **14**, 055001 (2012), URL http://stacks.iop.org/1367-2630/14/i=5/a=055001.

[23] T. Bienaimé, R. Bachelard, N. Piovella, and R. Kaiser, Fortschritte der Physik **61**, 377 (2013), https://onlinelibrary.wiley.com/doi/pdf/10.1002/prop.201200089, URL https://onlinelibrary.wiley.com/doi/abs/10.1002/prop.201200089.

[24] B. Zhu, J. Cooper, J. Ye, and A. M. Rey, Phys. Rev. A **94**, 023612 (2016), URL https://link.aps.org/doi/10.1103/PhysRevA.94.023612.

[25] S. D. Jenkins, J. Ruostekoski, J. Javanainen, R. Bourgain, S. Jennewein, Y. R. P. Sortais, and A. Browaeys, Phys. Rev. Lett. **116**, 183601 (2016), URL https://link.aps.org/doi/10.1103/PhysRevLett.116.183601.

[26] L. Corman, J. L. Ville, R. Saint-Jalm, M. Aidelsburger, T. Bienaimé, S. Nascimbène, J. Dalibard, and J. Beugnon, Phys. Rev. A **96**, 053629 (2017), URL https://link.aps.org/doi/10.1103/PhysRevA.96.053629.

[27] A. Fioretti, A. Molisch, J. Müller, P. Verkerk, and M. Allegrini, Optics Communications **149**, 415 (1998), ISSN 0030-4018, URL http://www.sciencedirect.com/science/article/pii/S0030401897007049.

[28] G. Labeyrie, D. Delande, C. Müller, C. Miniatura, and R. Kaiser, Optics Communications **243**, 157 (2004), ISSN 0030-4018, ultra Cold Atoms and Degenerate Quantum Gases, URL http://www.sciencedirect.com/science/article/pii/S0030401804010612.

[29] G. Labeyrie, R. Kaiser, and D. Delande, Applied Physics B **81**, 1001 (2005), ISSN 1432-0649, URL https://doi.org/10.1007/s00340-005-2015-y.

[30] T. Bienaimé, S. Bux, E. Lucioni, P. W. Courteille, N. Piovella, and R. Kaiser, Phys. Rev. Lett. **104**, 183602 (2010), URL https://link.aps.org/doi/10.1103/PhysRevLett.104.183602.

[31] J. Chabé, M.-T. Rouabah, L. Bellando, T. Bienaimé, N. Piovella, R. Bachelard, and R. Kaiser, Phys. Rev. A **89**, 043833 (2014), URL https://link.aps.org/doi/10.1103/PhysRevA.89.043833.

[32] C. E. Máximo, R. Bachelard, and R. Kaiser, Phys. Rev. A **97**, 043845 (2018), URL https://link.aps.org/doi/10.1103/PhysRevA.97.043845.

[33] W. Guerin, M. O. Araújo, and R. Kaiser, Phys. Rev. Lett. **116**, 083601 (2016), URL https://link.aps.org/doi/10.1103/PhysRevLett.116.083601.

[34] M. O. Araújo, I. Kresic, R. Kaiser, and W. Guerin, Phys. Rev. Lett. **117**, 073002 (2016), URL https://link.aps.org/doi/10.1103/PhysRevLett.117.073002.

[35] S. J. Roof, K. J. Kemp, M. D. Havey, and I. M. Sokolov, Phys. Rev. Lett. **117**, 073003 (2016), URL https://link.aps.org/doi/10.1103/PhysRevLett.117.073003.

[36] R. Romain, D. Hennequin, and P. Verkerk, The European Physical Journal D **61**, 171 (2011), ISSN 1434-6060, 1434-6079, URL https://link.springer.com/article/10.1140/epjd/e2010-00260-y.

[37] D. H. E. Dubin and T. M. O'Neil, Reviews of Modern Physics **71**, 87 (1999), URL https://link.aps.org/doi/10.1103/RevModPhys.71.87.

[38] H. Terças and J. Mendonça, Physical Review A **88**, 023412 (2013).

[39] R. Romain, H. Louis, P. Verkerk, and D. Hennequin, Physical Review A **89**, 053425 (2014), URL https://link.aps.org/doi/10.1103/PhysRevA.89.053425.

[40] J.-P. Hansen and I. R. McDonald, *Theory of simple liquids (Third Edition)* (Elsevier, 2006).

[41] M. H. Anderson, W. Petrich, J. R. Ensher, and E. A. Cornell, Phys. Rev. A **50**, R3597 (1994), URL https://link.aps.org/doi/10.1103/PhysRevA.50.R3597.

[42] D. W. Sesko, T. G. Walker, and C. E. Wieman, J. Opt. Soc. Am. B **8**, 946 (1991), URL http://josab.osa.org/abstract.cfm?URI=josab-8-5-946.

[43] G. L. Gattobigio, T. Pohl, G. Labeyrie, and R. Kaiser, Physica Scripta **81**, 025301 (2010), ISSN 1402-4896, URL http://stacks.iop.org/1402-4896/81/i=2/a=025301.

[44] G. L. Gattobigio, Phd thesis, Università degli studi di Ferrara ; Université Nice Sophia Antipolis (2008), URL https://tel.archives-ouvertes.fr/tel-00312718/document.

[45] L. Pruvost, in *AIP Conference Proceedings* (AIP, 2012), vol. 1421, pp. 80–92.

[46] H. Yoshida, Physics Letters A **150**, 262 (1990).

[47] W. R. Klein and B. D. Cook, IEEE Transactions on Sonics and Ultrasonics **14**, 123 (1967), ISSN 0018-9537.

[48] D. W. L. Sprung and J. Martorell, Journal of Physics A: Mathematical and General **30**, 6525 (1997), ISSN 0305-4470, URL http://stacks.iop.org/0305-4470/30/i=18/a=026.